Muon fluxes and showers from dark matter annihilation in the Galactic center

Arif Emre Erkoca,[1] Graciela Gelmini,[2] Mary Hall Reno,[3] and Ina Sarcevic[1,4]
[1]*Department of Physics, University of Arizona, Tucson, Arizona 85721, USA*
[2]*Department of Physics and Astronomy, University of California, Los Angeles, California 90095, USA*
[3]*Department of Physics and Astronomy, University of Iowa, Iowa City, Iowa 52242, USA*
[4]*Department of Astronomy and Steward Observatory, University of Arizona, Tucson, Arizona 85721, USA*
(Received 21 February 2010; published 25 May 2010)

We calculate contained and upward muon flux and contained shower event rates from neutrino interactions, when neutrinos are produced from annihilation of the dark matter in the Galactic center. We consider model-independent direct neutrino production and secondary neutrino production from the decay of taus, W bosons, and bottom quarks produced in the annihilation of dark matter. We illustrate how muon flux from dark matter annihilation has a very different shape than the muon flux from atmospheric neutrinos. We also discuss the dependence of the muon fluxes on the dark matter density profile and on the dark matter mass and of the total muon rates on the detector threshold. We consider both the upward muon flux, when muons are created in the rock below the detector, and the contained flux when muons are created in the (ice) detector. We also calculate the event rates for showers from neutrino interactions in the detector and show that the signal dominates over the background for 150 GeV $< m_\chi <$ 1 TeV for $E_{\rm sh}^{\rm th} =$ 100 GeV.

DOI: 10.1103/PhysRevD.81.096007 PACS numbers: 95.35.+d, 14.60.Lm, 95.55.Vj, 95.85.Ry

I. INTRODUCTION

Dark matter's presence is inferred from gravitational effects on visible matter at astronomical scales. A wide range of observational data show that the dark matter is cold or warm (i.e. it became nonrelativistic before or at the time of galaxy formation) and composes about 23% of the total density of the Universe [1]. There are no viable candidates for dark matter within the standard model of elementary particles, but many in proposed extensions of the standard model. Among these, weakly interacting massive particles (WIMPs) of mass in the 100 GeV to several TeV range provide a natural explanation for the observed dark matter density [2]. We are going to concentrate on WIMPs in this paper.

Although the detection of dark matter particles may be possible at the Large Hadron Collider (LHC), finding them in direct or indirect dark matter searches will be necessary to determine if they are indeed stable on cosmological time scales and how abundant they are at present [3]. Many direct or indirect dark matter searches are being carried on at present [4]. Indirect dark matter searches look for WIMP annihilation (or sometimes decay) products, either photons [5–7] or anomalous cosmic rays, such as positrons and antiprotons [8–14], or neutrinos [15–17]. For some years, observations of an excess in the positron fraction $e^+/(e^+ + e^-)$ by the High Energy Antimatter Telescope (HEAT) [9], a bright 511 keV gamma-ray line from the Galactic center by the International Gamma Ray Astrophysics Laboratory (INTEGRAL) [6], and a possible unaccounted-for component of the foreground of WMAP around the Galactic center, the ''WMAP haze'' [7] (among others) have been considered possible hints of WIMP dark matter annihilations.

More recently, the PAMELA satellite (Payload of Antimatter Matter Exploration and Light-nuclei Astrophysics (PAMELA) satellite reported an excess in the positron fraction in the energy range of 10–100 GeV with respect to what is expected from cosmic rays secondaries [10], which confirmed the HEAT excess. Also the Advanced Thin Ionization Calorimeter (ATIC) and the Polar Patrol Balloon and Balloon Borne Electron Telescope with Scintillating fibers (PPB-BETS) observed a bump in the $e^+ + e^-$ flux from 200 to 800 GeV [11,12], but this was not confirmed by the air Cherenkov telescope HESS [13] nor by the Fermi gamma ray telescope. Fermi found a slight excess in the $e^+ + e^-$ flux between 200 GeV and 1 TeV [14].

Indirect searches for dark matter annihilations via neutrinos with experiments such as the Antarctic Muon and Neutrino Detector Array (AMANDA) [15] and IceCube [16] also constrain dark matter models. The cubic kilometer size neutrino telescope (KM3NeT), planned to be built at the bottom of the Mediterranean Sea [17], will provide additional constraints, with its different view of the sky and, in particular, the Galactic center. Many theoretical studies have concentrated on the indirect dark matter detection via neutrino signals [18–22].

The positron excess observed by PAMELA may be explained by the presence of particular astrophysical sources (e.g., pulsars) [23], or by the annihilation [24,25] or decay [26] of dark matter particles. If the observed anomalies in the PAMELA and Fermi data are due to dark matter annihilation, a larger annihilation rate than expected for typical thermal relics must be assumed. This enhancement may happen due to either large inhomogeneities in the dark matter distribution near Earth (subhalos)

and/or a larger annihilation cross section of the dark matter particles. This last possibility may happen if the dark matter particles are not thermal relics [4,25], in which case they can have larger annihilation cross sections in the early Universe, or due to an enhancement of the annihilation cross section only at very low velocities [27], which would not affect their annihilation in the early Universe. Whatever its origin may be, the needed enhancement is quantified by a "boost factor," B, ranging from 10 to 10^4 [2,20–22]. The typical WIMP thermal relic annihilation cross section is $\langle\sigma v\rangle = 3 \times 10^{-26}\ \mathrm{cm}^3\,\mathrm{s}^{-1}$.

WIMP models explaining the PAMELA positron excess must be peculiar in other aspects as well. To avoid overproduction of antiprotons, the dark matter annihilation or decay must proceed dominantly to leptons. Moreover, the absence of a sharp shoulder in the electron plus positron spectrum (that had been observed by ATIC) in the Fermi data corresponding to an energy close to the parent dark matter particle mass means that the direct production of electrons must be suppressed with respect to the production of electrons (and positrons) as secondaries. Final states including τ's or μ's of dark matter not lighter than 1 TeV fit the PAMELA, HESS, and Fermi data best [28]. These leptophilic dark matter candidates [24] would copiously produce neutrinos [19] whose fluxes are constrained by the observations of Super Kamiokande [29] toward the direction of the Galactic center. Neutrinos with energies of the order of the dark matter mass, $E_\nu \leq m_\chi$, would propagate without being deflected toward the Earth. However, during their travel, vacuum oscillation effects would mix the three flavors. Some fraction of the arriving muon neutrinos would be converted into muons via charged-current interactions in the Earth which can be detected in Earth based neutrino telescopes.

Neutrino signals in underground or underwater detectors of dark matter annihilation in the Galactic center are the subject of this paper. We calculate the neutrino induced upward and contained muon flux, as well as the neutrino induced muon and shower event rates due to dark matter annihilation in the Galactic center. We take into account the muon propagation in the Earth when evaluating the upward muon flux [30] and study the energy range of muons for which upward muon events dominate over the contained ones. We show that the shape of upward muon fluxes differs significantly from the shape of the neutrino spectra at production, due to the smearing produced by neutrino interactions and muon propagation. The muon propagation shifts the flux to lower energies, while the contained muon flux increases with muon energy due to the linear energy dependence of the neutrino charged-current interaction. We consider different WIMPs annihilation channels that contribute to the neutrino signal, including direct annihilation to neutrinos, to charged leptons and to quarks or gauge bosons. We evaluate rates of contained events and upward events, of relevance to IceCube and future neutrino detectors like KM3NeT.

In the next section, we evaluate expressions for muon flux from the incident neutrino flux interacting with the medium. In Sec. III we present our results for muon flux and muon event rates from the annihilation of the dark matter in the Galactic center compared with the atmospheric background and evaluate rates for hadronic and electromagnetic showers. Finally, in Sec. IV we summarize and discuss our results.

II. MUON FLUX

The neutrino flux at the Earth due to the annihilation of dark matter particles with mass m_χ in the Galactic center is given by

$$\frac{d\phi_\nu}{dE_\nu} = R \times \left(\sum_F B_F \frac{dN_\nu^F}{dE_\nu}\right), \tag{1}$$

where R is the annihilation rate given by

$$R = B\frac{\langle\sigma v\rangle}{8\pi m_\chi^2}\int d\Omega \int_{\mathrm{l.o.s.}} dl(\theta)\rho^2(l), \tag{2}$$

where dN_ν^F/dE_ν is the neutrino spectrum at the production for a given annihilation channel F with branching fraction B_F, B is the boost factor, $\rho(l)$ is the dark matter density, the integral is over the line of sight (l.o.s.) within a solid angle $\Delta\Omega$, centered in the Galactic center. The neutrino energy distribution, dN_ν^F/dE_ν, depends on the particle produced. Some examples appear in Appendix A. For all of the evaluations below, we take the dark matter annihilation cross section to have the typical thermal relic value $\langle\sigma v\rangle = 3 \times 10^{-26}\ \mathrm{cm}^3\,\mathrm{s}^{-1}$.

For practical reasons the dimensionless quantity $\langle J_2\rangle_\Omega$ is defined in which the dark matter density profile $\rho(l)$ is embedded [19],

$$\langle J_2\rangle_\Omega = \int \frac{d\Omega}{\Delta\Omega}\int_{\mathrm{l.o.s.}} \frac{dl(\theta)}{R_o}\left(\frac{\rho(l)}{\rho_o}\right)^2, \tag{3}$$

where $l(\theta)$ is the distance from us in the direction of θ which is the cone half angle from the Galactic center, R_o is the distance of the solar system from the Galactic center, and ρ_o is the local density near the Solar System, which are taken to be $R_o = 8.5$ kpc and $\rho_o = 0.3\ \mathrm{GeV\,cm}^{-3}$. As a practical matter, we consider two profiles, the Navarro-Frenk-White (NFW) [31] profile and a cored isothermal profile. Some typical values for $\langle J_2\rangle_\Omega\Delta\Omega$ can be found in Ref. [32], where $\langle J_2\rangle_\Omega\Delta\Omega = 6.0(10.0)$ for $\theta = 5^\circ(10^\circ)$ for the NFW profile, and $\langle J_2\rangle_\Omega\Delta\Omega = 1.3(4.3)$ with $\theta = 5^\circ(10^\circ)$ for the isothermal profile.

The high energy neutrinos coming from the Galactic center then interact with the matter in the Earth and produce muons that traverse to the detector (upward events), or they interact in the detector producing muons or showers (contained events). Muon range or stopping distance, $R_\mu(E_\mu^i, E_{\mathrm{th}})$, is given by

$$R_\mu(E^i_\mu, E_{\rm th}) = \frac{1}{\beta\rho}\log\left(\frac{\alpha+\beta E^i_\mu}{\alpha+\beta E_{\rm th}}\right), \quad (4)$$

where α corresponds to the ionization energy loss and β accounts for the bremsstrahlung, pair production, and photonuclear interactions. For example, for a muon with initial energy $E^i_\mu \sim 1$ TeV, when $E_{\rm th} = 1$ GeV the muon range is roughly 1 km whereas the decay length of a muon with the same initial energy is much larger ($\sim$ a few thousand kilometers). For detectors with a characteristic size of 1 km^3, contained events are most important for WIMP masses below about 1 TeV, while for smaller detectors like Super Kamiokande, upward events are relatively more important.

Using Eq. (1) and following the theoretical framework presented in Ref. [30], the upward muon flux at the detector is given by

$$\frac{d\phi_\mu}{dE_\mu} = \int_0^{R_\mu(E^i_\mu,E_\mu)} dz \int_{E^i_\mu}^{m_\chi} dE_\nu \left(\frac{d\phi_\nu}{dE_\nu}\right) P_{\rm surv}(E^i_\mu, E_\mu) \times \frac{dP_{CC}}{dz dE^i_\mu}\frac{dE^i_\mu}{dE_\mu} + (\nu \to \bar\nu). \quad (5)$$

Here $P_{\rm surv}$ accounts for muon energy loss in transit from its production position to the muon's entry into the detector. For an energy independent energy loss parameter β, the survival probability is

$$P_{\rm surv}(E^i_\mu, E_\mu) \simeq \left(\frac{E_\mu}{E^i_\mu}\right)^\Gamma \left(\frac{\alpha+\beta E^i_\mu}{\alpha+\beta E_\mu}\right)^\Gamma, \quad (6)$$

where $\Gamma = m_\mu/(c\tau_\mu \alpha\rho)$ in terms of the muon mass, muon lifetime, and the density of the medium ρ in g/cm^3.

For production in the detector, the contained muon flux is

$$\frac{d\phi_\mu}{dE^i_\mu} = \int_0^D dz \int_{E^i_\mu}^{m_\chi} dE_\nu \left(\frac{d\phi_\nu}{dE_\nu}\right)\frac{dP_{CC}}{dz dE^i_\mu} + (\nu \to \bar\nu), \quad (7)$$

where D is the size of the detector. The quantity dP_{CC} is the probability for a neutrino with energy E_ν to convert into a muon within the energy interval of dE^i_μ and over a distance dz:

$$dP_{CC} = dz dE^i_\mu \frac{N_A\rho}{2}\left(\frac{d\sigma^p_\nu(E_\nu, E^i_\mu)}{dE^i_\mu} + (p \to n)\right), \quad (8)$$

where $N_A = 6.022 \times 10^{23}$ is Avogadro's number. The differential cross sections $d\sigma^{p,n}_\nu/dE^i_\mu$ are the weak scattering cross sections of (anti-)neutrinos on the nucleons, which can be approximated by [33]

$$\frac{d\sigma^{p,n}_{\nu,\bar\nu}}{dE^i_\mu} = \frac{2m_p G_F^2}{\pi}\left(a^{p,n}_{\nu,\bar\nu} + b^{p,n}_{\nu,\bar\nu}\left(\frac{E^i_\mu}{E_{\nu,\bar\nu}}\right)^2\right). \quad (9)$$

The parameters a and b for charged-current scattering are shown in Table I.

TABLE I. Parameters for the charged-current neutrino-nucleon differential cross section, as noted in Ref. [33].

a^p_ν	0.15	b^p_ν	0.04
$a^p_{\bar\nu}$	0.04	$b^p_{\bar\nu}$	0.15
a^n_ν	0.25	b^n_ν	0.06
$a^n_{\bar\nu}$	0.06	$b^n_{\bar\nu}$	0.25

TABLE II. Parameters for the neutral-current neutrino-nucleon differential cross section, as noted in Ref. [33].

a^p_ν	0.058	b^p_ν	0.022
$a^p_{\bar\nu}$	0.019	$b^p_{\bar\nu}$	0.064
a^n_ν	0.064	b^n_ν	0.019
$a^n_{\bar\nu}$	0.022	$b^n_{\bar\nu}$	0.058

Muon rates, $N_\mu(m_\chi)$, are obtained by integrating Eqs. (5) and (7) over the muon energies, i.e.,

$$N_\mu(m_\chi) = \int_{E_{\rm th}}^{m_\chi} \frac{d\phi_\mu}{dE_\mu} dE_\mu, \quad (10)$$

where $E_{\rm th}$ is the muon detector threshold.

Another set of possible signals of dark matter are the showers produced in neutrino charged-current (CC) and neutral-current (NC) interactions in the detector. The contained shower flux in CC and NC interactions is given by [34]

$$\frac{d\phi}{dE_{\rm sh}} = \int_0^D dz \int_{E_{\rm sh}}^{m_\chi} dE_\nu \left(\frac{d\phi_\nu}{dE_\nu}\right)\frac{dP_{\rm CC(NC)}}{dz dE_{\rm sh}} + (\nu \to \bar\nu), \quad (11)$$

where the shower energy is

$$E_{\rm sh} \approx E_\nu - E_{\mu,\tau,e}. \quad (12)$$

The neutral-current cross section can also be approximated with Eq. (9) where the parameters a and b appear in Table II.

In the limit of the survival probability $P_{\rm surv}$ going to unity, the energy dependent flux can be calculated analytically when Eq. (9) is used for the neutrino-nucleon cross section. The analytic results for a variety of decay channels are shown in Appendix B.

III. RESULTS

The direct production channel, $\chi\chi \to \nu_\mu\bar\nu_\mu$, where χ is the WIMP, is the most promising channel for the detection of dark matter annihilation, assuming an adequate annihilation cross section, because of the monoenergetic neutrinos. A typical example of a dark matter particle candidate which annihilates into a neutrino pair is the lightest Kaluza-Klein particle. However, some particle candidates, for example, neutralinos and leptophilic dark matter, produce neutrinos only as secondary particles, via the decay of

the particles into which the dark matter particles annihilate, such as $\mu^+\mu^-$, $\tau^+\tau^-$, $b\bar{b}$, W^+W^-, etc.

In Figs. 1 and 2, we present our results for the differential upward muon flux due to the annihilation of a dark matter particle via the direct production ($\chi\chi \to \nu_\mu \bar{\nu}_\mu$) channel. To illustrate various contributions, we choose the dark matter particle mass $m_\chi = 500$ GeV, and for Fig. 1, the NFW dark matter density profile [31] and the boost factor $B = 200$ which is in the range of the boost factor values that explain the PAMELA data [21]. For Fig. 2, the dark matter density profile is the cored isothermal profile and we use a boost factor $B = 800$ to match the normalization of the NFW density profile for the 5° cone half angle.

We show our results for two different choices of the cone half angle (5° and 10°) and compare them with the angle-averaged background due to the atmospheric neutrinos (in units of $\mathrm{GeV}^{-1}\,\mathrm{km}^{-2}\,\mathrm{yr}^{-1}\,\mathrm{sr}^{-1}$)

$$\left(\frac{d\phi_\nu}{dE_\nu d\Omega}\right)_{\mathrm{ATM,avg}} = N_0 E_\nu^{-\gamma-1}\left(\frac{a}{bE_\nu}\ln(1+bE_\nu) + \frac{c}{eE_\nu}\ln(1+eE_\nu)\right), \tag{13}$$

which was obtained using the angle-dependent atmospheric neutrino flux parametrization in Ref. [35],

$$\frac{d\phi_\nu}{dE_\nu d\Omega} = N_0 E_\nu^{-\gamma-1}\left(\frac{a}{1+bE_\nu\cos\theta} + \frac{c}{1+eE_\nu\cos\theta}\right). \tag{14}$$

The values of the parameters N_0, γ, a, b, c, and e, given in Table III, were determined by fitting angle-dependent atmospheric neutrino data from Ref. [36]. The resulting final muon flux with this approximated neutrino background is about 50% larger (smaller) than that from the vertical (horizontal) atmospheric neutrinos.

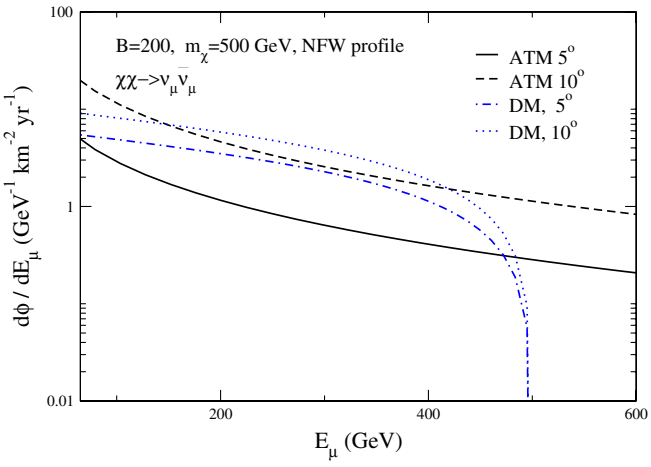

FIG. 1 (color online). Upward muon flux obtained from dark matter annihilation into neutrinos in the Galactic center, for a cone half angle (θ) of 5° (dot-dashed curve) and 10° (dotted curve). The background upward muon fluxes due to (angle-averaged) atmospheric neutrinos are shown with the solid (for $\theta = 5°$) and the dashed (for $\theta = 10°$) curves. The NFW dark matter profile is used, along with a boost factor $B = 200$ and $m_\chi = 500$ GeV.

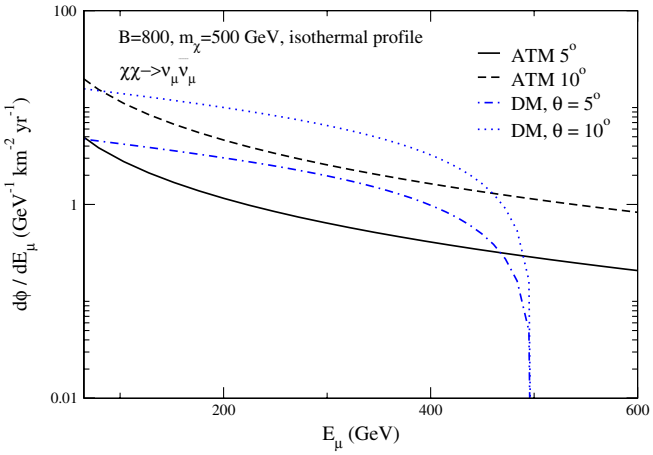

FIG. 2 (color online). Same as Fig. 1 but for the cored isothermal dark matter density profile and a boost factor $B = 800$.

For a 10° cone half angle, the signal dominates over the background in the range $180\ \mathrm{GeV} < E_\mu < 420\ \mathrm{GeV}$ for the NFW profile. We note that the background signal is suppressed more than the dark matter signal with the decrease in the cone of half angle. As a comparison, for a 5° cone half angle the signal exceeds the background in a wider range of energies, $60\ \mathrm{GeV} < E_\mu < 480\ \mathrm{GeV}$.

From Fig. 2, we note that in the case of the isothermal profile for the dark matter in which there is a relatively less dense core region in the isothermal profile, by increasing the cone half angle from 5° to 10°, there is an almost equal enhancement of the upward muon fluxes from the atmospheric neutrino background and from the dark matter annihilation in the center of the galaxy. For the set of parameters that we choose here, the dark matter signal becomes larger than the background in the energy ranges of $100\ \mathrm{GeV} < E_\mu < 470\ \mathrm{GeV}$ and $70\ \mathrm{GeV} < E_\mu < 480\ \mathrm{GeV}$ for the cone half angles 10° and 5°, respectively.

Figure 3 shows the dependence of the differential muon fluxes from dark matter annihilation via the direct production channel for $m_\chi = 200$, 500, and 800 GeV. We again

TABLE III. Parameters for the atmospheric ν_μ and $\bar{\nu}_\mu$ flux, in units of $\mathrm{GeV}^{-1}\,\mathrm{km}^{-2}\,\mathrm{yr}^{-1}\,\mathrm{sr}^{-1}$.

γ	1.74
a	0.018
b	0.024 GeV^{-1}
c	0.0069
e	0.001 39 GeV^{-1}
N_0	1.95×10^{17} for ν
	1.35×10^{17} for $\bar{\nu}$.

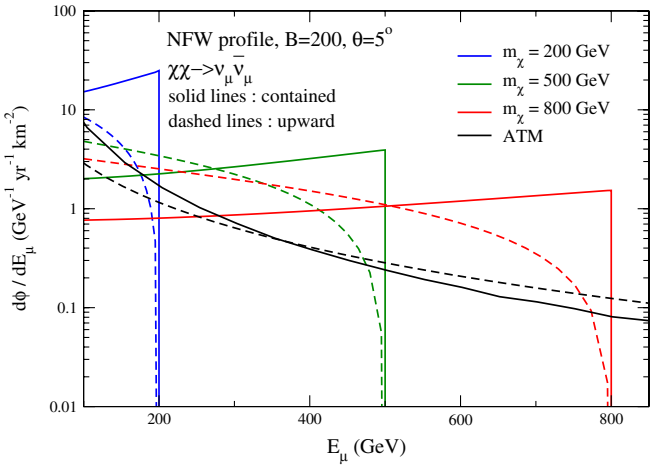

FIG. 3 (color online). Muon flux due to the dark matter annihilation into neutrinos in the Galactic center for different dark matter masses; curves correspond to the dark matter masses of 200, 500, and 800 GeV, respectively. The corresponding backgrounds are also shown. All the solid lines correspond to the contained events with $D = 1$ km, whereas the dashed ones to upward events.

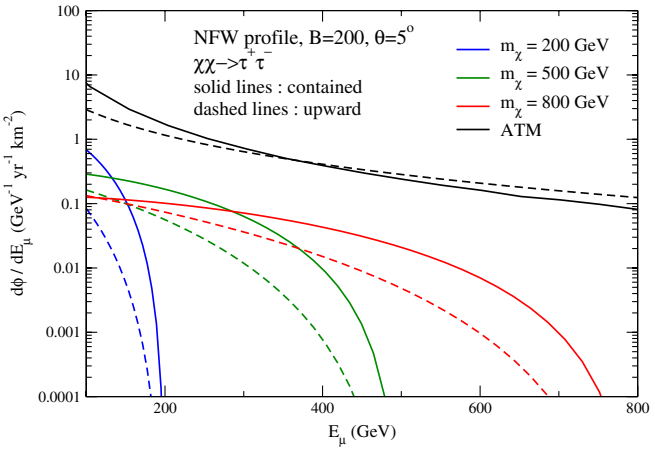

FIG. 4 (color online). Muon fluxes due to the secondary neutrinos produced through the dark matter annihilation into tau particles in the Galactic center for different dark matter masses; $m_\chi = 200$, 500, and 800 GeV. The solid (dashed) curves correspond to contained (upward) events.

consider the NFW profile, a fixed boost factor ($B = 200$) and a fixed cone half angle ($\theta = 5°$). The figure shows the upward flux as well as the contained flux assuming a detector size $D = 1$ km in Eq. (7). We find that regardless of the mass dependence, the upward event spectrum is a decreasing function of the muon energy whereas the corresponding spectrum of the contained events increases with the muon energy up to the cutoff set by the initial neutrino energy. In our calculations, we assume that the dark matter particles annihilate at rest and thus the neutrino energy for this decay mode can be set to the rest mass of the dark matter particle, $E_\mu = m_\chi$.

The signal for the muon flux from the contained events has a stronger suppression with the increase in the dark matter mass than for the upward muon events. This is due to the m_χ^{-2} dependence in Eq. (2). The mass dependence for upward events is more complex because of the mass dependence in the upper limit of the z integration in Eq. (5). A large mass m_χ (and therefore higher E_ν) produces a higher energy muon which has a longer range in the rock below the detector. For example, for $E_\mu >$ 380 GeV, the upward event signal from the annihilation of the dark matter particle with mass $m_\chi = 800$ GeV dominates over the one from that of the dark matter particle with mass $m_\chi = 500$ GeV.

For a wide range of muon energies, the dark matter signal is above the atmospheric background both for contained and upward events in the $\chi\chi \to \nu_\mu \bar{\nu}_\mu$ channel with the boost factor used here. We find that for a given dark matter mass the contained events exceed the upward ones in the range $E_\mu \geq 0.6 m_\chi$.

In Fig. 4, we present our results for the differential muon flux due to the $\chi\chi \to \tau^+\tau^-$ channel. This channel is characteristic of all three-body decays into neutrinos (secondary neutrinos). Again shown are the upward and contained signals from $m_\chi = 200$, 500, and 800 GeV with the NFW profile and $B = 200$.

Note that in the case of secondary neutrinos, the signals for both upward and contained events decrease as the muon energy increases, and for a fixed m_χ, the contained events, in general, dominate over the upward events for muon energies 100 GeV $\leq E_\mu \leq m_\chi$. This is a consequence of considering a detector size of $D = 1$ km, a size larger than the range of a muon with an energy of less than 1 TeV. The figure shows that even for a half angle of 5°, in the case of a NFW profile one would need a boost factor on the order of about 2000 for the dark matter signals from the secondary neutrinos to be above the atmospheric background.

Measurement of the muon flux can also be used to distinguish different dark matter models, as seen in Fig. 5 where we compare signals from different annihilation channels: $\chi\chi \to W^+W^-$, $\chi\chi \to \tau^+\tau^-$, and $\chi\chi \to b\bar{b}$ for the NFW profile, with $B = 200$, the half angle equal to 5°, and $m_\chi = 500$ GeV. The signals from the b quark and the tau decay modes differ only by an overall factor which is close to the ratio of the decay branching fractions of the corresponding modes given in Appendix A. However, for the W decay, being a 2-body decay, the shape of the differential muon spectrum is quite different than those of the b quark and tau which are both 3-body decay modes. This indicates that muon flux from the secondary neutrinos as a by-product of the dark matter annihilation can also be useful in discriminating different dark matter models.

We now turn to the total rate of upward and contained muons produced by $\nu_\mu + \bar{\nu}_\mu$ from direct dark matter

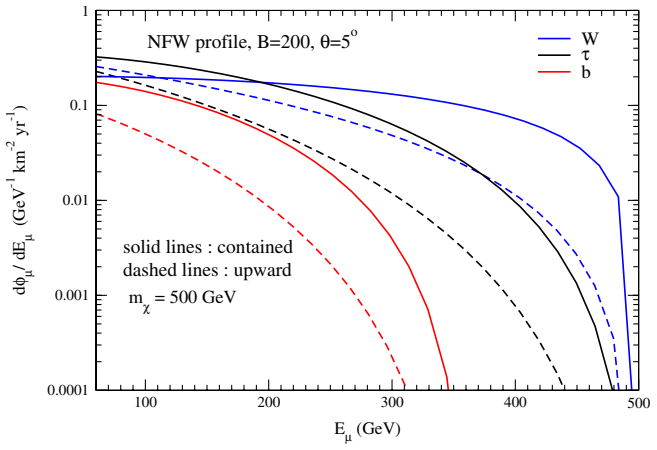

FIG. 5 (color online). Muon fluxes due to the secondary neutrinos produced through the dark matter annihilation into W bosons (upper curves), tau particles (middle curves), and bottom quarks (lower curves) in the Galactic center. The solid (dashed) lines for each channel correspond to contained (upward) events. The detector size is taken to be $D = 1$ km, and the cone half angle is $\theta = 5^\circ$ for the NFW profile with $B = 200$.

annihilation to neutrinos. Integrating the differential fluxes over the final muon energy, we obtain the muon rate from the annihilation of the dark matter as a function of the mass m_χ (Fig. 6) for the NFW profile with $B = 200$ and $\theta = 5^\circ$. Here, the threshold energy is taken to be $E_{\rm th} = 80$ GeV. Because of the finite size of the detector ($D = 1$ km), and m_χ^{-2} dependence of the annihilation rate, the signal for the contained events decreases with increasing the dark matter mass. On the other hand for upward events, heavier dark matter particles yield more energetic neutrinos which makes a larger portion of muons in the rock below the detector to contribute to the final muon flux. This effect combined with the energy dependence of the neutrino charged-current cross section results in an increasing muon rate up to $m_\chi = 650$ GeV, at which point the m_χ^{-2} dependence of the annihilation rate takes over resulting in a slow decrease of the muon rate. Comparison of contained and upward muon rates presented in Fig. 6 indicates that for $m_\chi \leq 500$ GeV the signal from the contained events still dominates over the signal from the upward events. Even though the signal depends weakly on the value of the threshold energy, the background is very sensitive to it due to the large contribution from the low energy atmospheric neutrinos. The signal-to-background ratio increases with increasing the muon energy threshold. We obtain the same results for the isothermal dark matter density halo profile if the boost factor is taken to be 800 for the same cone half angle of 5°.

In Fig. 7 we show our results for the 10° cone half angle. We note that in the case of contained events the signal dominates over the background for 100 GeV $\leq m_\chi \leq$ 200 GeV, when the threshold energy is 80 GeV. For upward events, the signal is below the background for all m_χ. The isothermal dark matter density halo profile gives a larger signal than obtained with the NFW profile by about a factor of 2, due to its larger increase of $\langle J_2 \rangle_\Omega$ for 10° relative to 5°.

In Fig. 8 we show contour plots for upward muon events, $N_\mu = (0.5, 5, 50, 500, 850)$ km^{-2} yr^{-1}. The solid (dashed) lines correspond to the muon energy threshold of 50 (80) GeV. We also calculate that $N_\mu = 714(516)$ km^{-2} yr^{-1} for the upward muon events due to the atmospheric muon neutrinos for the muon energy threshold of 50 (80) GeV. We find that for a fixed cone half angle the annihilation cross section does not depend on m_χ for $m_\chi > 200$ GeV to produce a given total muon flux since the decrease in the annihilation rate with m_χ is compensated with the increase in the muon range and neutrino cross section with m_χ. The dependence on the choice of the threshold is also negligible. However, for low

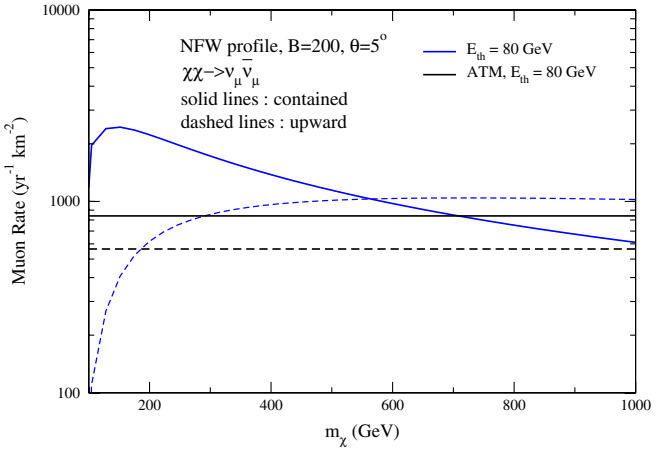

FIG. 6 (color online). Total muon fluxes due to the dark matter annihilation into neutrinos in the Galactic center. The solid (dashed) lines correspond to contained (upward) events. Atmospheric background is presented with horizontal lines.

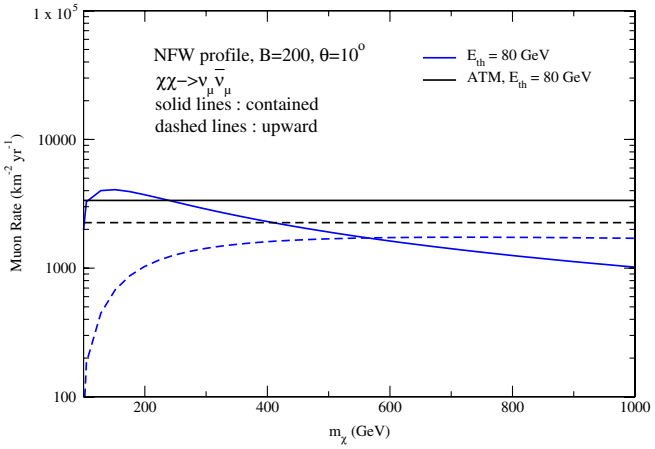

FIG. 7 (color online). Same as Fig. 6 but for a 10° cone half angle.

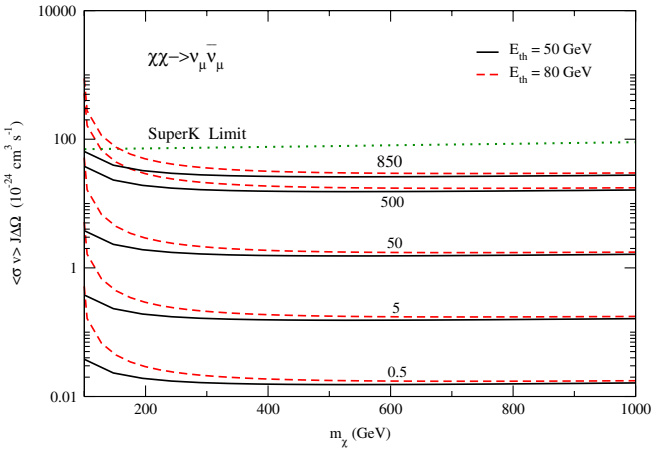

FIG. 8 (color online). Upward muon events curves, $N_\mu = (0.5, 5, 50, 500, 850)\ \mathrm{km}^{-2}\,\mathrm{yr}^{-1}$, for the energy threshold of 50 and 80 GeV are shown by the solid and the dashed lines, respectively. The boost factor is set to be unity and the cone half angle is chosen to be 5°.

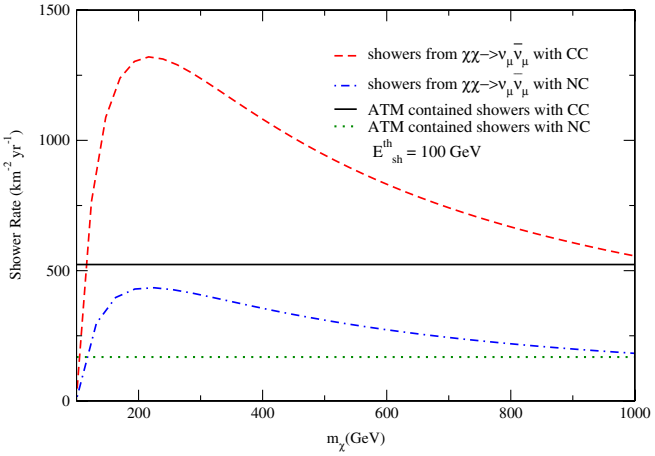

FIG. 9 (color online). Hadronic shower rates for charged-current (dashed curve) and neutral-current (dot-dashed curve) interactions of $\nu_\mu + \bar{\nu}_\mu$ when muon neutrinos are produced directly from the dark matter annihilation in the Galactic center, compared with the atmospheric background. The NFW profiles with $B = 200$, $\theta = 5°$, and $D = 1$ km are used.

mass dark matter particles, higher values of the annihilation cross sections are required in order to have the same total muon flux. This is due to the fact that the neutrinos originated from this low mass dark matter annihilation mostly contribute to the muon flux at energies less than the thresholds we choose. The parameter space above the dotted line is excluded at 90% C.L. by Super Kamiokande observations toward the direction of the Galactic center with a cone half angle of 5° [29].

The dominant atmospheric neutrino flavor at neutrino energies above 40 GeV is ν_μ which produces tracklike events through charged-current interactions in the neutrino telescopes. Identifying tracklike events could reduce the background substantially. Recently it has been argued that IceCube+DeepCore will be able to put constraints on dark matter properties in a more efficient way by just analyzing the cascade (i.e. shower) events which are due to charged-current interactions of $\nu_{e,\tau}$ and the neutral-current interactions of all of the neutrino flavors [22]. Since the weak scattering cross sections are independent of the flavors, the signal-to-background ratio is enhanced in shower events since ν_μ can only contribute to the shower events through neutral-current interactions where the cross section is about $1/3$ of the charged-current cross section.

In Fig. 9, we show hadronic shower rates as a function of m_χ from neutral-current and charged-current interactions of muon neutrinos and antineutrinos. These rates are the same for any other neutrino flavor with a democratic $\chi\chi \to \nu\bar{\nu}$ annihilation rate. Also shown is the hadronic shower rate due to the atmospheric muon neutrinos: $N_{\mathrm{sh}}^{\mathrm{atm}} = 524(168)\ \mathrm{km}^{-2}\,\mathrm{yr}^{-1}$ for the charged-current (neutral-current) interactions. The shower threshold is taken to be 100 GeV. We note that the background due to the atmospheric electron and tau neutrinos is much smaller than for the muon neutrinos, so the signal to background would not change much here when all the neutrino flavors were included.

We also evaluate the electromagnetic shower rate as a function of m_χ due to electrons produced by the charged-current interactions of ν_e, with an electromagnetic shower threshold set at 100 GeV. The atmospheric shower rate is evaluated using the atmospheric ν_e and $\bar{\nu}_e$ fluxes for an effective zenith angle $0.4 < \cos\theta_z < 0.5$, which roughly corresponds to the angle describing the position of the Galactic center relative to the IceCube,

$$\left(\frac{d\phi}{dEd\Omega}\right)_{\nu_e} = \frac{500.0}{(\mathrm{GeV\,m^2\,s\,sr})}\left(\frac{E}{\mathrm{GeV}}\right)^{-3.57},$$
$$\left(\frac{d\phi}{dEd\Omega}\right)_{\bar{\nu}_e} = \frac{382.6}{(\mathrm{GeV\,m^2\,s\,sr})}\left(\frac{E}{\mathrm{GeV}}\right)^{-3.57}. \quad (15)$$

From Fig. 10 we see that the signal-to-background ratio is increased for the electromagnetic showers relative to hadronic showers (see Fig. 9) mainly due to a very small atmospheric electron neutrino flux which is about $34\ \mathrm{km}^{-2}\,\mathrm{yr}^{-1}$. For secondary electron neutrinos from the decay of taus which are produced via $\chi\chi \to \tau^+\tau^-$, the signal becomes comparable to the background.

For the future neutrino detector which is positioned in the northern hemisphere, such as KM3Net, the relevant background would be coming from almost horizontal showers, which is about a factor of 3 to 4 times larger than the flux given by Eq. (14), giving approximately an electromagnetic shower flux of $100\ \mathrm{km}^{-2}\,\mathrm{yr}^{-1}$.

In Figs. 11 and 12, we present the contour plots for contained showers with the energy threshold of 100 GeV. The main difference between the showers and the upward muons appears for $m_\chi > 200$ GeV where for a given total

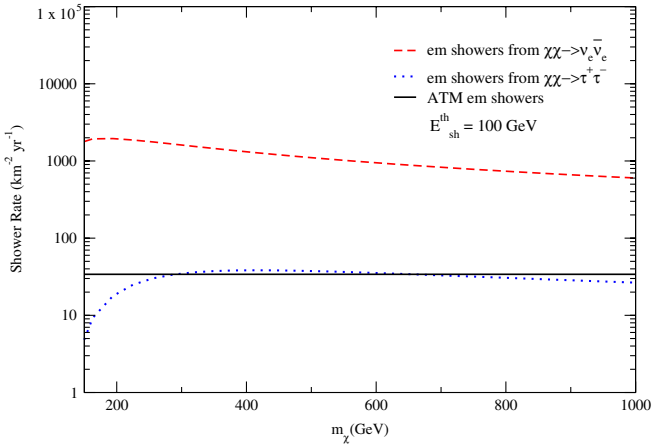

FIG. 10 (color online). Electromagnetic shower rates as a function of m_χ for $\nu_e + \bar{\nu}_e$ charged-current interactions when electron neutrinos are produced directly in the annihilation of dark matter in the Galactic center, compared with the atmospheric background for shower energies above 100 GeV. The NFW profiles with $B = 200$, $\theta = 5°$, and $D = 1$ km are used.

number of shower events higher annihilation cross sections is required with the increase in m_χ. This is due to the contained event nature of the shower events which are all produced inside the detector with finite size. Thus, in contrast to the case for the upward muon events that we discussed earlier, the strong suppression of the annihilation rate with m_χ cannot be compensated because of the finite size of the detector. The charged-current showers actually require smaller annihilation cross sections in order to produce the same number of total shower events that neutral-current showers produce for a fixed m_χ due to the larger weak scattering cross sections.

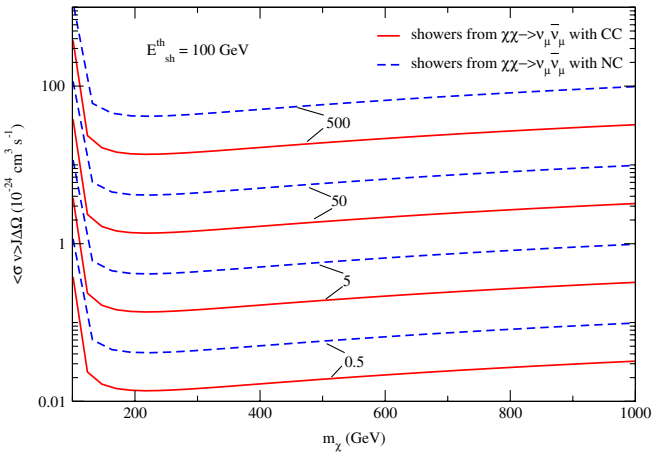

FIG. 11 (color online). Hadronic shower event curves, $N^h_{\rm sh} = (0.5, 5, 50, 500)$ km^{-2} yr^{-1}, for the charged-current (solid curves) and neutral-current (dashed curves) processes, for a NFW dark matter density profile, a 5° cone half angle, the boost factor set to be unity, and $D = 1$ km.

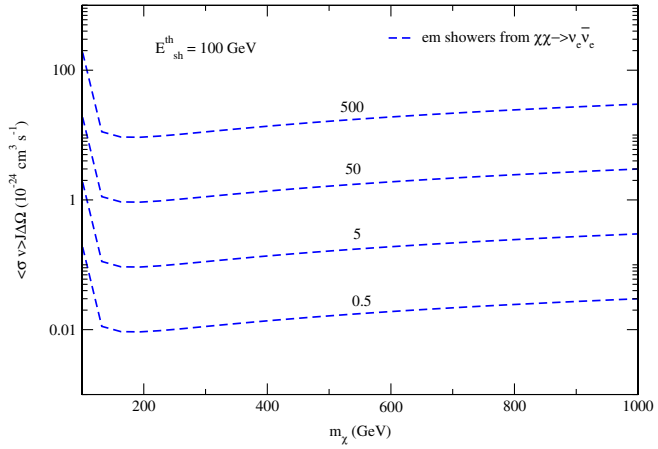

FIG. 12 (color online). Electromagnetic shower event curves, $N^{\rm em}_{\rm sh} = (0.5, 5, 50, 500)$ km^{-2} yr^{-1} for a NFW dark matter density profile, a 5° cone half angle, the boost factor set to be unity, and $D = 1$ km.

The signal detection significance can be evaluated using

$$S = \frac{N_s}{\sqrt{(N_s + N_b)}}, \tag{16}$$

where N_s corresponds to the number of events for the signal, while N_b is the background. We obtain the time it would take to observe a 5σ effect using our results for the contained muon events (Fig. 6), hadronic showers (Fig. 9), and electromagnetic showers (Fig. 10),

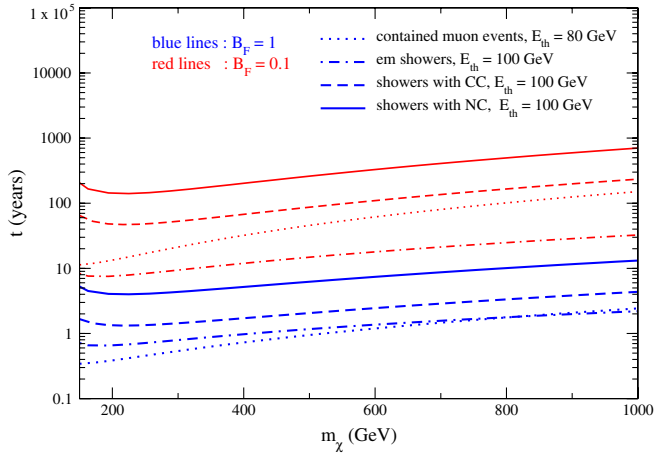

FIG. 13 (color online). Time as a function of dark matter mass, m_χ, for the direct neutrino production channel ($\chi\chi \rightarrow \nu\bar{\nu}$) to reach a 5σ detection level for the IceCube+DeepCore detector. The curves correspond to hadronic showers (solid for neutral-current, dashed for charged-current interactions), electromagnetic showers (dotted curves) and the contained muon events (dot-dashed curves). $B_F = 1(0.1)$ for the lower (upper) curves, the boost factor is taken to be 200, and the cone half angle is 5° for all curves.

$$t = \frac{25(N_s + N_b)}{N_s^2 V}, \tag{17}$$

where $V = 0.04(0.02)$ km^3 is the effective volume of IceCube+DeepCore for the tracklike (shower) events. In Fig. 13, we show the observation time (t) required for IceCube+DeepCore detector to detect or exclude the dark matter signal via the direct production channel at a 5σ level. Here, we again use a fixed boost factor ($B = 200$) and cone half angle ($\theta = 5°$). Our results, when we take $B_F = 1$ for the direct production channel, suggest that in less than 2 years of observation IceCube+DeepCore will be able to reach a 5σ detection for the contained muon and electromagnetic shower events for a wide range of m_χ. Decreasing the branching fraction by an order of magnitude increases the observation time significantly in order to reach the same significance. For instance, $t \simeq$ 10–50 yr, for 150 GeV $\geq m_\chi \leq$ 500 GeV in the case of contained muon events, and somewhat shorter for the electromagnetic showers.

In the case of secondary neutrino production, when neutrinos are produced from tau decays, and taus are products of dark matter annihilation, these neutrinos can interact inside the detector producing hadronic and electromagnetic showers, in addition to muon neutrinos producing muons via charge-current interactions. In Fig. 14 we show that the IceCube+DeepCore detector could potentially detect a 2σ effect in 5 (8) yr for $m_\chi =$ 300 GeV (1 TeV), in the case of excluding muonlike events. To reach a 2σ detection for the electromagnetic showers due to the secondary electron neutrinos IceCube +DeepCore will need about 10–20 yr of observation for

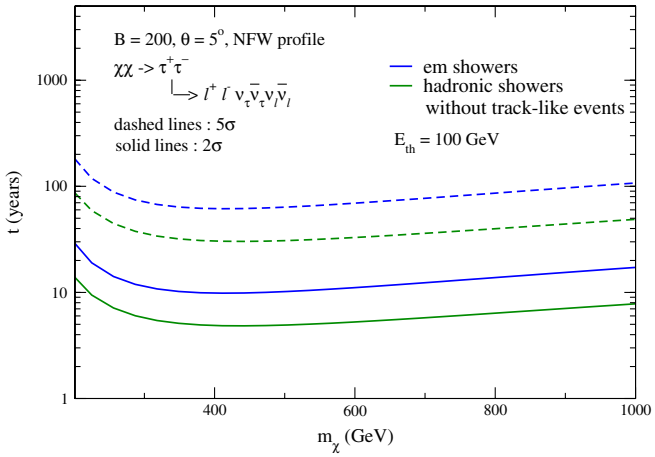

FIG. 14 (color online). Time as a function of dark matter mass, m_χ, for the secondary neutrino production channel $\chi\chi \rightarrow \tau^+\tau^- \rightarrow l^+l^-\nu_\tau\bar{\nu}_\tau\nu_l\bar{\nu}_l$ to reach a 2σ (solid curves) or a 5σ (dashed curves) detection level when measuring electromagnetic showers (top curves) and hadronic showers without charged tracklike events (lower curves).

250 GeV $\leq m_\chi \leq$ 1 TeV. When muonlike events are included, the observation times for the hadronic showers become similar to those for the electromagnetic showers. The time needed for a 5σ effect for hadronic (electromagnetic) showers is almost an order of magnitude longer than for a 2σ effect.

Comparing the secondary and direct production (Fig. 13) one sees that it takes longer (by about 1 order of magnitude) to detect showers from secondary neutrinos than to detect showers from primary neutrinos. This is because of the different shape of the shower energy distributions: for direct neutrinos it increases with energy and for secondary neutrinos it decreases with energy.

Since the angular resolution for showers is expected to be much worse than for muons, for the angular resolution of 30°, the number of signal events will be larger by a factor of 6, while the background will increase by a factor of 35, which results in reducing the time it would take IceCube+DeepCore to see a 2σ effect to 3 yr for hadronic showers without tracklike events. This is in qualitative agreement with the results presented in Ref. [37].

For dark matter models in which neutrinos are decay products of taus produced in the dark matter annihilation, looking for contained hadronic showers in IceCube +DeepCore seems promising to detect a signal at the 2σ level, assuming the NFW dark matter halo profile and a boost factor $B = 200$.

In Table IV we give a summary of our results for the event rates for various dark matter masses. We consider the direct production of neutrinos ($\chi\chi \rightarrow \nu\bar{\nu}$) and the neutrinos from the tau decay ($\chi\chi \rightarrow \tau^+\tau^- \rightarrow l^+l^-\nu_\tau\bar{\nu}_\tau\nu_l\bar{\nu}_l$). We classify the event rates as contained (ct) and upward (up) for the tracklike muon (μ) events, and depending on the type of the interaction involved, charged current (CC), neutral current (NC), and electromagnetic (em) for the shower events. Two different cone half angles are chosen, $\theta = 5°$ and $\theta = 10°$, and the threshold energies for the tracklike muon (shower) events are set to be 80 (100) GeV. We also show the atmospheric neutrino background for the tracklike muon and for the shower events.

IV. CONCLUSION

We have studied neutrino signals from dark matter annihilation in the Galactic center. We have calculated contained and upward muon fluxes from neutrino interactions, when neutrinos are produced in annihilation of dark matter either directly or via the decay of taus, W bosons, or b quarks. We have shown that in the case of direct neutrino production, the signal is above the atmospheric background for both contained and upward events, assuming that the annihilation rate is enhanced by a boost factor of 200 (when the NFW dark matter halo profile is used) and that the branching ratio of dark matter annihilation into neutrinos is 1. In general, the boost factor values that are required to explain the data obtained by

TABLE IV. Event rates per km^2 per yr for the contained (ct), upward (up) muons (μ), and for the showers (sh) produced via charged-current (CC), neutral-current (NC), and electromagnetic (em) interactions. Neutrinos from direct production ($\chi\chi \to \nu\bar{\nu}$) channel and secondary neutrinos from $\chi\chi \to \tau^+\tau^-$ channel are considered. We have set $B \cdot B_F = 200$ for each channel. The cone half angle is chosen to be 5° and 10°. The threshold energy for the muon (shower) events is set to be 80 (100) GeV. The backgrounds due to atmospheric neutrinos are also presented.

	m_χ (GeV)								
	200	300	400	500	600	700	800	900	1000
$\chi\chi \to \nu\bar{\nu}$									
$N^{\mu}_{\rm ct}(5°)$	2240	1750	1385	1135	976	850	750	670	611
$N^{\mu}_{\rm ct}(10°)$	3808	2975	2355	1930	1659	1445	1275	1139	1039
$N^{\mu}_{\rm up}(5°)$	615	850	960	1010	1035	1042	1040	1033	1023
$N^{\mu}_{\rm up}(10°)$	1046	1445	1632	1717	1760	1771	1768	1756	1739
$N^{\rm NC}_{\rm sh}(5°)$	430	400	355	310	274	240	220	200	182
$N^{\rm NC}_{\rm sh}(10°)$	731	680	604	527	466	408	374	340	309
$N^{\rm CC}_{\rm sh}(5°)$	1310	1230	1080	935	830	741	665	605	556
$N^{\rm CC}_{\rm sh}(10°)$	2227	2091	1836	1590	1411	1260	1131	1029	945
$N^{\rm em}_{\rm sh}(5°)$	1920	1600	1300	1100	950	820	730	660	600
$N^{\rm em}_{\rm sh}(10°)$	3264	2720	2210	1870	1615	1394	1241	1122	1020
$\chi\chi \to \tau^+\tau^-$									
$N^{\rm NC}_{\rm sh}(5°)$	17	28	33	33	32	31	28	27	24
$N^{\rm NC}_{\rm sh}(10°)$	29	48	56	56	54	53	48	46	41
$N^{\rm CC}_{\rm sh}(5°)$	39	66	73	72	70	66	61	58	55
$N^{\rm CC}_{\rm sh}(10°)$	66	112	124	122	119	112	104	99	94
$N^{\rm em}_{\rm sh}(5°)$	20	34	38	37	35	33	31	29	27
$N^{\rm em}_{\rm sh}(10°)$	34	58	65	63	60	56	53	49	46
$\mathrm{ATM}^{\mu}_{\rm ct}$	839 (5°)				3356 (10°)				
$\mathrm{ATM}^{\mu}_{\rm up}$	564 (5°)				2256 (10°)				
$\mathrm{ATM}^{\rm NC}_{\rm sh}$	169 (5°)				676 (10°)				
$\mathrm{ATM}^{\rm CC}_{\rm sh}$	523 (5°)				2092 (10°)				
$\mathrm{ATM}^{\rm em}_{\rm sh}$	34 (5°)				136 (10°)				

the indirect detection experiments vary depending on the dark matter model and the dark matter mass. For the specific dark matter model our results can be rescaled by the corresponding product of the boost factor B and the branching ratio B_F.

We have found that the contained muon flux dominates over the upward muon flux for all energies when $m_\chi = 200$ GeV. However, as we increase the mass m_χ of the dark matter particle, for example, when $m_\chi = 500$ GeV, the upward muon flux dominates up to $E_\mu = 300$ GeV, and for $m_\chi = 800$ GeV, up to $E_\mu = 500$ GeV. This is due to the increasing muon range as the muon initial energy increases, which becomes possible when m_χ is larger, thus producing higher energy neutrinos in the annihilation. In the case of secondary neutrino production, the signal becomes comparable to the background if the boost factor is an order of magnitude larger than the value we considered. We have shown that the shape of the muon flux depends on the specific decay mode, and that the dominant flux comes from tau decay at low muon energies, and from W decay for muon energies above 200 GeV. The total upward muon rates have a weak dependence on m_χ and on the muon energy threshold for $m_\chi > 400$ GeV, due to the balance of the energy dependence of the muon range, the upper limit of the muon energy (given by m_χ) and the explicit dependence on m_χ ($\sim m_\chi^{-2}$) of the muon flux. However, the total contained muon rates show a sharp decrease with m_χ for $m_\chi > 150$ GeV due to the finite size of the detector. Upward muon events dominate over contained muon events for $m_\chi > 550$ GeV.

We have also shown that showers produced by neutrino interactions, when neutrinos are produced directly in dark matter annihilation, could also be used to detect a dark matter signal from the Galactic center. In particular, electromagnetic showers have much smaller background, from atmospheric electron neutrinos, than the hadronic showers. In addition, we have studied the contour plots of both the upward muon events and the showers and we have shown the required dependence of the annihilation cross section on the dark matter mass in order to observe a fixed number of event rates. We have discussed the origin of different shapes for the contour curves in each case and pointed out the contained event nature of the shower events. We have shown that after 1 yr the IceCube +DeepCore detector could potentially observe a 5σ signal effect by measuring contained muons (for direct neutrino

production), or in 5 to 8 yr a 2σ effect with hadronic showers even in the case when they are due to secondary neutrinos.

IceCube+DeepCore will be able to identify tracklike events due to the charged-current interactions of muon neutrinos, the showers due to neutral-current interactions of all the neutrino flavors, and the charged-current interactions of electron and tau neutrinos. In particular, above the neutrino energy of 40 GeV the signal-to-background ratio for showers is further enhanced since the atmospheric tau and electron neutrino fluxes are suppressed relative to the atmospheric muon neutrino flux. Thus, the main background is the neutral-current interaction whose cross section is about a factor of 3 less than the charged-current cross section of the atmospheric muon neutrinos. The measurement of the ratio of tracklike muon and shower events eliminates the dependence on some parameters of the theory (e.g., boost factor, the dark matter density profile, etc.) which only determine the overall normalization for the energy dependent differential muon fluxes, so the physical properties of the dark matter particle can better be determined.

In addition to the boost factor due to Sommerfeld enhancement that we have considered, there is potential enhancement of the dark matter signal due to the existence of small substructures in the Milky Way halo [38]. Possible observation of this additional boost may be difficult to observe because of the small population of these substructures unless the neutrino detectors have a very good angular resolution [20].

Because of its location in the northern hemisphere, the future KM3NeT experiment will be complementary to IceCube+DeepCore in searching for neutrino signals from dark matter annihilation in the Galactic center through the observation of upward muon events. The atmospheric muon background at the KM3NeT will be suppressed significantly since the Earth will act as a shield to those muons. Independent searches of the upward muon events by KM3NeT and the contained muon and shower events by IceCube+DeepCore look promising for the discovery of the mysterious dark matter particle or for setting stringent constraints on its properties.

ACKNOWLEDGMENTS

We would like to thank Tyce DeYoung, Sven Lafebre, Irina Mocioiu, Anna Stasto, and Tolga Guver for useful discussions. I. S. and G. G. would like to thank the Aspen Center for Physics, where part of this work took place. This research was supported by the U.S. Department of Energy Contracts No. DE-FG02-91ER40664, No. DE-FG02-04ER41319, and No. DE-FG02-04ER41298. G. G. was supported in part by the U.S. Department of Energy Grant No. DE-FG03-91ER40662, Task C at UCLA.

APPENDIX A: NEUTRINO ENERGY DISTRIBUTIONS

1. Neutrino energy distribution from direct production

The neutrino energy distribution when neutrinos are produced directly from dark matter annihilation is given by a delta function,

$$\frac{dN_\nu}{dE_\nu} = \delta(E_\nu - m_\chi), \tag{A1}$$

where the assumption is that the dark matter particles are essentially at rest when they annihilate.

2. Neutrino energy distribution from $\tau^+\tau^-$ and $b\bar{b}$ decay modes

In these decay modes, we use the unpolarized decay distributions, so the ν and $\bar{\nu}$ distributions are assumed to be the same. The decay branching fraction is denoted by B_f for a given decay mode f, $f = \tau, b$. The b quarks hadronize before they decay into neutrinos. The hadronization effect is taken into account by scaling the initial quark energy, $E_{\rm in} = m_\chi$, in the form $E_f = z_f m_\chi$, where $z_f = 0.73$ for b quarks [39].

The neutrino energy distribution from the decay of $f = \tau^+, \tau^-, b$, or $\bar{b}$ from $\chi\chi \to f\bar{f}$ is approximately

$$\frac{dN_\nu}{dE_\nu} = \frac{2B_f}{E_f}(1 - 3x^2 + 2x^3), \quad \text{where } x = \frac{E_\nu}{E_f} \le 1, \tag{A2}$$

where for each neutrino or antineutrino flavor (ν_e, $\bar{\nu}_e$, ν_μ, $\bar{\nu}_\mu$),

$$(E_f, B_f) = \begin{cases} (m_\chi, 0.18) & \tau \text{ decay}, \\ (0.73 m_\chi, 0.103) & b \text{ decay}. \end{cases} \tag{A3}$$

The energy distribution of the tau neutrinos from the decay of $f = b$ or $\bar{b}$ is given by (A2) and the distribution from the decay of τ^+ or τ^- is given by [34]

$$\frac{dN_{\nu_\tau}}{dE_{\nu_\tau}} = \frac{4B_f}{3E_f}(1 - x^3), \quad \text{where } x = \frac{E_{\nu_\tau}}{E_f} \le 1. \tag{A4}$$

3. W^+W^- decay mode

In the W^+W^- mode, when the dark matter particle is at rest when it annihilates, $E_W = m_\chi/2$ and $\beta_W = \sqrt{1 - m_W^2/m_\chi^2}$. The decay distribution, for each W, is

$$\frac{dN_\nu}{dE_\nu} = \frac{B}{m_\chi \beta_W} \quad \text{with}$$
$$\frac{m_\chi}{2}(1 - \beta_W) < E_\nu < \frac{m_\chi}{2}(1 + \beta_W). \tag{A5}$$

Here, $B = 0.105$ for each neutrino flavor.

APPENDIX B: MUON ENERGY DISTRIBUTION

The differential muon flux for the $\chi\chi \to \nu\bar{\nu}$ channel can be given as

$$\frac{d\phi_\mu}{dE_\mu} = \frac{c}{m_\chi^2(E_\mu + \alpha/\beta)}\left[a(m_\chi - E_\mu) + \frac{b}{3m_\chi^2}(m_\chi^3 - E_\mu^3)\right], \tag{B1}$$

where

$$c = B\frac{R_o\rho_o^2 B_F\langle\sigma v\rangle_F\langle J_2\rangle_\Omega \Delta\Omega m_p G_F^2 N_A}{4\pi^2\beta}. \tag{B2}$$

There is a separate distribution for neutrino and antineutrinos, since the parameters a and b depend on the incident particle and the target. Here, for isoscalar nucleon targets, $a = a_{\nu,\bar{\nu}} = 0.20,\ 0.05$ and $b = b_{\nu,\bar{\nu}} = 0.05,\ 0.20$. Also appearing are the Fermi constant $G_F \simeq 1.17 \times 10^{-5}$ GeV^{-2} and Avogadro's number $N_A \simeq 6 \times 10^{23}$. For standard rock, $\alpha \simeq 2 \times 10^{-3}$ GeV cm^2/g accounts for the ionization energy loss and $\beta \simeq 3.0 \times 10^{-6}$ cm^2/g accounts for the bremsstrahlung, pair production, and photonuclear interactions and we take $\rho = 2.6$ cm^3/g.

For the contained events, a similar expression can be derived as

$$\frac{d\phi_\mu}{dE_\mu} = \frac{c'}{m_\chi^2}\left(a + b\frac{E_\mu^2}{m_\chi^2}\right)\Theta(m_\chi - E_\mu), \tag{B3}$$

where $\Theta(x) = 1$ if $x \geq 0$ and $\Theta(x) = 0$ otherwise, and

$$c' = DB\frac{R_o\rho_o^2 B_F\langle\sigma v\rangle_F\langle J_2\rangle_\Omega \Delta\Omega m_p G_F^2 N_A \rho}{4\pi^2}, \tag{B4}$$

where D is the size of the detector.

We note that

$$\frac{d\phi_\mu}{dE_\mu} \propto \rho^0 \text{ for the upward events,}$$

$$\frac{d\phi_\mu}{dE_\mu} \propto \rho^1 \text{ for the contained events,}$$

so, the muon flux does not depend on the rock density for the upward events except through α and β, whereas for the contained events, the muon flux is directly proportional to the density of the medium.

All the expressions for the muon flux derived below contain a $\Theta(m_\chi - E_\mu)$ function. For secondary neutrinos which possess an energy spectrum in the form

$$\left(\frac{dN}{dE}\right)_\nu = A\left(\frac{E_\nu}{m_\chi}\right)^n, \tag{B5}$$

where A is an overall factor, the differential upward muon flux can be calculated by using

$$\frac{d\phi_\mu}{dE_\mu} = \frac{cA}{m_\chi^{(n+2)}(E_\mu + \frac{\alpha}{\beta})}[P(m_\chi, E_\mu, n) + K(m_\chi, E_\mu, n) + L(m_\chi, E_\mu, n) + M(m_\chi, E_\mu, n)], \tag{B6}$$

where

$$\begin{aligned} P(m_\chi, E_\mu, n) &= \frac{am_\chi^{(n+1)}(m_\chi - E_\mu)}{(n+1)}, \\ K(m_\chi, E_\mu, n) &= -\frac{a(m_\chi^{(n+2)} - E_\mu^{(n+2)})}{(n+1)(n+2)}, \\ L(m_\chi, E_\mu, n) &= \frac{bm_\chi^{(n-1)}(m_\chi^3 - E_\mu^3)}{3(n-1)}, \\ M(m_\chi, E_\mu, n) &= -\frac{b(m_\chi^{(n+2)} - E_\mu^{(n+2)})}{(n-1)(n+2)}, \end{aligned} \tag{B7}$$

for $n \neq 1$ and when $n = 1$,

$$\frac{d\phi_\mu}{dE_\mu} = \frac{cA}{3m_\chi^3(E_\mu + \frac{\alpha}{\beta})}\left[m_\chi^3\left(a + \frac{b}{3}\right) - \frac{3aE_\mu m_\chi^2}{2} + E_\mu^3\left(b\ln\left(\frac{E_\mu}{m_\chi}\right) + \frac{a}{2} - \frac{b}{3}\right)\right]. \tag{B8}$$

For the contained events and when $n \neq 1$,

$$\frac{d\phi_\mu}{dE_\mu} = \frac{c'A}{m_\chi^{(n+2)}}\left[\frac{a}{(n+1)}(m_\chi^{(n+1)} - E_\mu^{(n+1)}) + \frac{bE_\mu^2}{(n-1)}(m_\chi^{(n-1)} - E_\mu^{(n-1)})\right], \tag{B9}$$

which reduces to

$$\frac{d\phi_\mu}{dE_\mu} = \frac{c'A}{m_\chi^3}\left[\frac{a}{2}(m_\chi^2 - E_\mu^2) + bE_\mu^2\ln\left(\frac{m_\chi}{E_\mu}\right)\right] \tag{B10}$$

when $n = 1$.

[1] See, e.g., J. Einasto, arXiv:0901.0632, and references therein.

[2] See, e.g., L. Bergstrom, New J. Phys. **11**, 105006 (2009), and references therein.

[3] D. Hooper and E. A. Baltz, Annu. Rev. Nucl. Part. Sci. **58**, 293 (2008).

[4] See, e.g., G. B. Gelmini, Int. J. Mod. Phys. A **23**, 4273 (2008), and references therein.

[5] W. B. Atwood *et al.* (Fermi/LAT Collaboration), Astrophys. J. **697**, 1071 (2009); E. O. Wilhelmi (HESS Collaboration), AIP Conf. Proc. **1112**, 16 (2009); M. Beilicke (VERITAS Collaboration), AIP Conf. Proc. **1112**, 33 (2009); T. Mizukami (CANGAROO-III Collaboration), AIP Conf. Proc. **1085**, 364 (2008); Y. Yukawa (CANGAROO Collaboration), J. Phys. Conf. Ser. **120**, 062018 (2008); J. Rico *et al.* (MAGIC Collaboration), AIP Conf. Proc. **1112**, 23 (2009).

[6] P. Jean *et al.*, Astron. Astrophys. **407**, L55 (2003); C. Boehm, D. Hooper, J. Silk, M. Casse, and J. Paul, Phys. Rev. Lett. **92**, 101301 (2004).

[7] D. P. Finkbeiner, Astrophys. J. **614**, 186 (2004); G. Dobler and D. P. Finkbeiner, Astrophys. J. **680**, 1222 (2008); M. Bottino, A. J. Banday, and D. Maino, arXiv:0807.1865; D. Hooper, D. P. Finkbeiner, and G. Dobler, Phys. Rev. D **76**, 083012 (2007).

[8] M. Aguilar *et al.* (AMS-01 Collaboration), Phys. Lett. B **646**, 145 (2007); C. Goy (AMS Collaboration), J. Phys. Conf. Ser. **39**, 185 (2006); D. Casadei, arXiv:0609072.

[9] S. W. Barwick *et al.* (HEAT Collaboration), Astrophys. J. **482**, L191 (1997).

[10] O. Adriani *et al.* (PAMELA Collaboration), Nature (London) **458**, 607 (2009); E. Mocchiutti *et al.*, arXiv:0905.2551.

[11] J. Chang *et al.*, Nature (London) **456**, 362 (2008).

[12] S. Torii *et al.* (PPB-BETS Collaboration), arXiv:0809.0760; K. Yoshida *et al.*, Adv. Space Res. **42**, 1670 (2008).

[13] H. E. S. Aharonian, Astron. Astrophys. **508**, 561 (2009).

[14] A. A. Abdo *et al.* (Fermi LAT Collaboration), Phys. Rev. Lett. **102**, 181101 (2009).

[15] J. Braun and D. Hubert (IceCube Collaboration), arXiv:0906.1615; D. Hubert (IceCube Collaboration), Nucl. Phys. B, Proc. Suppl. **173**, 87 (2007).

[16] R. Abbasi *et al.* (IceCube Collaboration), Nucl. Instrum. Methods Phys. Res., Sect. A **601**, 294 (2009); C. Rott (IceCube Collaboration), arXiv:0810.3698.

[17] U. F. Katz (KM3NeT Collaboration), Nucl. Instrum. Methods Phys. Res., Sect. A **602**, 40 (2009).

[18] See, e.g., P. Gondolo and J. Silk, Phys. Rev. Lett. **83**, 1719 (1999); D. Hooper and G. D. Kribs, Phys. Rev. D **67**, 055003 (2003); G. Bertone, E. Nezri, J. Orloff, and J. Silk, Phys. Rev. D **70**, 063503 (2004).

[19] J. Hisano, M. Kawasaki, K. Kohri, and K. Nakayama, Phys. Rev. D **79**, 043516 (2009).

[20] J. Liu, P. F. Yin, and S. H. Zhu, Phys. Rev. D **79**, 063522 (2009).

[21] D. Spolyar, M. Buckley, K. Freese, D. Hooper, and H. Murayama, arXiv:0905.4764; I. Cholis, L. Goodenough, D. Hooper, M. Simet, and N. Wiener, Phys. Rev. D **80**, 123511 (2009).

[22] M. R. Buckley, K. Freese, D. Hooper, D. Spolyar, and H. Murayama, Phys. Rev. D **81**, 016006 (2010).

[23] A. M. Atoian, F. A. Aharonian, and H. J. Volk, Phys. Rev. D **52**, 3265 (1995); D. Hooper, P. Blasi, and P. D. Serpico, J. Cosmol. Astropart. Phys. 01 (2009) 025; P. D. Serpico, Phys. Rev. D **79**, 021302 (2009); H. Yuksel, M. D. Kistler, and T. Stanev, Phys. Rev. Lett. **103**, 051101 (2009); S. Profumo, arXiv:0812.4457; P. Blasi and P. D. Serpico, Phys. Rev. Lett. **103**, 081103 (2009); P. Mertsch and S. Sarkar, Phys. Rev. Lett. **103**, 081104 (2009).

[24] See, e.g., P. J. Fox and E. Poppitz, Phys. Rev. D **79**, 083528 (2009); R. Harnik and G. D. Kribs, Phys. Rev. D **79**, 095007 (2009); Q. H. Cao, E. Ma, and G. Shaughnessy, Phys. Lett. B **673**, 152 (2009); B. Kyae, J. Cosmol. Astropart. Phys. 07 (2009) 028; X. J. Bi, X. G. He, and Q. Yuan, Phys. Lett. B **678**, 168 (2009); S. Baek and P. Ko, J. Cosmol. Astropart. Phys. 10 (2009) 011; D. J. Phalen, A. Pierce, and N. Wiener, Phys. Rev. D **80**, 063513 (2009); H. S. Goh, L. J. Hall, and P. Kumar, J. High Energy Phys. 05 (2009) 097; A. Ibarra, A. Ringwald, D. Tran, and C. Weniger, J. Cosmol. Astropart. Phys. 08 (2009) 017.

[25] See, e.g., G. Kane, R. Lu, and S. Watson, Phys. Lett. B **681**, 151 (2009).

[26] See, e.g., E. Nardi, F. Sannino, and A. Strumia, J. Cosmol. Astropart. Phys. 01 (2009) 043; A. Arvanitaki, S. Dimopoulos, S. Dubovsky, P. W. Graham, R. Harnik, and S. Rajendran, Phys. Rev. D **80**, 055011 (2009); A. Ibarra, D. Tran, and C. Weniger, J. Cosmol. Astropart. Phys. 01 (2010) 009.

[27] A. Sommerfeld, Ann. Phys. (Leipzig) **403**, 257 (1931); J. Hisano, S. Matsumoto, and M. M. Nojiri, Phys. Rev. Lett. **92**, 031303 (2004); N. Arkani-Hamed, D. P. Finkbeiner, T. R. Slatyer, and N. Weiner, Phys. Rev. D **79**, 015014 (2009); I. Cholis, G. Dobler, D. P. Finkbeiner, L. Goodenough, and N. Weiner, Phys. Rev. D **80**, 123518 (2009); J. M. Russell, S. M. West, D. Cumberbatch, and D. Hooper, J. High Energy Phys. 07 (2008) 058; J. M. Russell and S. M. West, Phys. Lett. B **676**, 133 (2009).

[28] P. Meade, M. Papucci, A. Strumia, and T. Volansky, Nucl. Phys. **B831**, 178 (2010); V. Barger, Y. Gao, W. Y. Keung, D. Marfatia, and G. Shaughnessy, Phys. Lett. B **678**, 283 (2009).

[29] S. Desai *et al.* (Super-K Collaboration), Phys. Rev. D **70**, 083523 (2004); **70**, 109901(E) (2004).

[30] A. E. Erkoca, M. H. Reno, and I. Sarcevic, Phys. Rev. D **80**, 043514 (2009).

[31] J. F. Navarro, C. S. Frenk, and S. D. M. White, Astrophys. J. **462**, 563 (1996).

[32] J. Hisano, K. Nakayama, and Masaki J. S. Yang, Phys. Lett. B **678**, 101 (2009).

[33] A. Strumia and F. Vissani, arXiv:0606054.

[34] S. I. Dutta, M. H. Reno, and I. Sarcevic, Phys. Rev. D **62**, 123001 (2000).

[35] T. K. Gaisser and M. Honda, Annu. Rev. Nucl. Part. Sci. **52**, 153 (2002).

[36] M. Honda, T. Kajita, K. Kasahara, S. Midorikawa, and T. Sanuki, Phys. Rev. D **75**, 043006 (2007).

[37] S. K. Mandal, M. R. Buckley, K. Freese, D. Spolyar, and H. Murayama, Phys. Rev. D **81**, 043508 (2010).

[38] M. Kamionkowski, S. M. Koushiappas, and M. Kuhlen, Phys. Rev. D **81**, 043532 (2010).

[39] G. Jungman and M. Kamionkowski, Phys. Rev. D **51**, 328 (1995); P. Lipari, Astropart. Phys. **1**, 195 (1993).